Pharmaceutical Research, Vol. 27, No. 5, May 2010 (© 2010)
DOI: 10.1007/s11095-009-0046-5

Research Paper

Classification of Annular Bed Flow Patterns and Investigation on Their Influence on the Bottom Spray Fluid Bed Coating Process

Li Kun Wang,[1] Paul Wan Sia Heng,[1] and Celine Valeria Liew[1,2]

Received August 13, 2009; accepted December 27, 2009; published online March 5, 2010

Purpose. This study aims to classify annular bed flow patterns in the bottom spray fluid bed coating process, study their influence on coat uniformity and investigate the feasibility of developing real-time annular bed flow pattern detection as a PAT tool.
Methods. High-speed imaging and particle image velocimetry were used to visualize annular bed flow. Color coating and subsequent tristimulus colorimetry were employed to determine influence of annular bed flow pattern on coat uniformity. Feasibility of monitoring annular bed flow pattern through an observation window was tested using miniaturized particle velocity field and time series particle velocity orientation information.
Results. Three types of annular bed flow patterns were identified. Plug flow gave the best coat uniformity followed by global and localized fluidization. Plug flow may be advantageous for high spray-rate conditions, large-scale coating and prevention of particle segregation. Plug flow could be differentiated from the other flow patterns through a simulated observation window.
Conclusion. Annular bed flow patterns were classified and found to influence particle coat uniformity noticeably. Availability of annular bed flow information for large-scale coaters would enable adjustments for process optimization. This study highlights the potential of monitoring annular bed flow pattern as a PAT tool.

KEY WORDS: annular bed flow pattern; bottom spray fluid bed coating; coat uniformity; particle image velocimetry; process analytical technology.

INTRODUCTION

Multi-particulate drug delivery systems have advantages of more uniform gastric transit time and less gastric irritation over conventional tablets (1). Coating of multi-particulates is important for modifying drug release profile, protecting encapsulated constituents from the environment, improving product appearance and enhancing product mechanical strength. Bottom spray fluid bed coating is the main method for coating multi-particulates.

Three main regions—central up-bed region, fountain region and annular down-bed region—can be identified based on different material movement patterns (2) in the bottom spray fluid bed coating process (Fig. 1-a). The air distribution plate design enables the air flow rate to be high in the partition column but lower in the annular down-bed region. This results in an air velocity which is higher than the terminal velocity of particles in the up-bed region, thus conveying particles through the spray zone upwards and out from the top of the partition column. In the fountain or deceleration region, air velocity drops to below terminal velocity, causing particles to decelerate and move downwards to the annular down-bed region. In this staging area, particles are held, moving downwards, awaiting re-entry through the partition gap into the partition column for another coating cycle. Studies carried out to date on the bottom spray fluid bed coating process focused mainly on finding correlations between the coating material and the degree of agglomeration, particle movement within the partition column (3), drying efficiency (4), coating apparatus modification (5) and particle cycle-time distribution (6–9). Although these studies gave a better understanding of the bottom spray fluid bed coating process, the quality by design (QbD) concept requires a systematic approach to be adopted to study the bottom spray fluid bed coating process by the use of an in-process monitoring tool.

Under the QbD framework, the variability sources in the bottom spray fluid bed coating process need to be quantified and controlled to ensure coat uniformity, which is considered a critical quality attribute of the coated product (10). Bottom spray fluid bed coating is a layering process, in which particles pass through the spray zone, partition column, fountain region and annular bed repetitively. Consequently, uniformly coated particles can be expected if particles repeat the coating cycle in an orderly manner. On the other hand, particle flow patterns that disrupt the coating cycle order result in higher inter-particle coat variability. Particle recirculation within the partition column, particle mass flow rate and annular bed

[1] GEA-NUS Pharmaceutical Processing Research Laboratory, Department of Pharmacy, National University of Singapore, 18 Science Drive 4, Singapore, 117543, Singapore.
[2] To whom correspondence should be addressed. (e-mail: phalcv@nus.edu.sg)

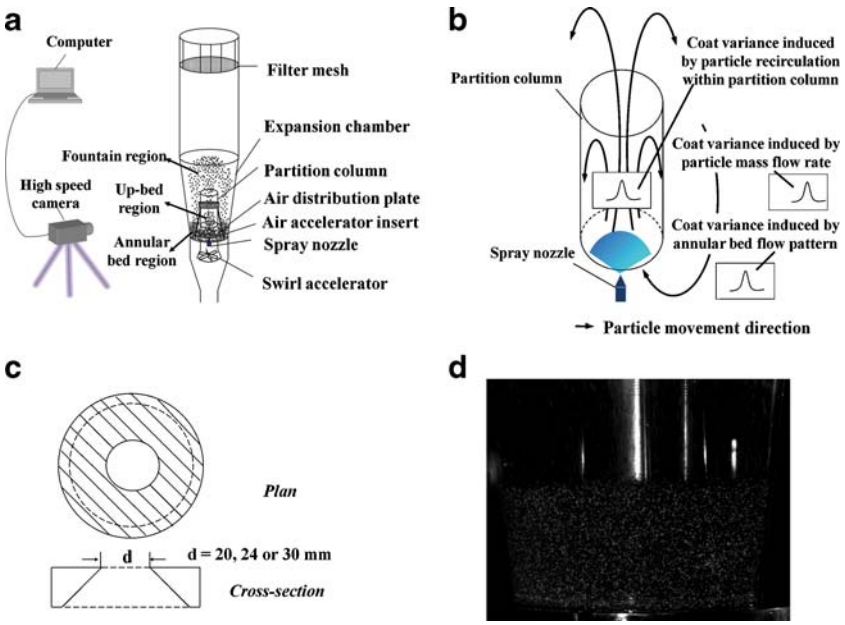

Fig. 1. (a) Apparatus set-up for video capture of annular bed flow pattern, indicating three main regions, up-bed region, fountain region and annular bed region; (b) schematic diagram of variability sources for bottom spray fluid bed coating (c) schematic diagram of air accelerator insert (AAI) with diameter of *d* mm; (d) sample high-speed image of annular bed flow.

flow pattern are the three main factors that can cause non-uniformity in the particle coat (Fig. 1-b). Particle recirculation within the partition column is considered the main source of process variability (11–13). This is because particles joining recirculation may not be fully dried as they may re-enter the spray zone in differing cycle times, resulting in agglomeration and non-uniform coating. A visiometric process analyzer has been developed for quantifying particle recirculation within the partition column (13). High speed photography revealed that particle recirculation within the partition column can be reduced by adding additional swirl air accelerator and air accelerator insert (AAI) to the Wurster coater (5). Particle mass flow rate affects coat uniformity by influencing the mean frequency of particles passing through the spray zone. Annular bed flow pattern affects coat uniformity by influencing the order of the particle "queue" in the staging region prior to their passing through the spray zone.

The influence of annular bed flow pattern on the bottom spray fluid bed coating has largely been neglected with few studies carried out on annular bed flow patterns. In previous studies, where only particle cycle-time distribution was considered, the influences of annular bed flow pattern were confounded by the effects of particle recirculation within the partition column and particle mass flow (2,6). Without experimental support, bubbling fluidization was described qualitatively and mathematically as the default annular bed flow pattern (2,14). As a result, the types and behavior of annular bed flow patterns remained unclear. Furthermore, the influence of annular bed flow pattern on particle coat uniformity has not been determined experimentally. Therefore, it was highly desirable to systematically study annular bed flow pattern and its possible influences on particle coating, particularly on coat uniformity. The primary objective of this study was to visualize, quantify and classify annular bed flow patterns. The secondary objective was to investigate the influences of different types of annular bed flow patterns on particle coat uniformity. The significance of annular bed flow patterns and the possibility of developing annular bed flow pattern detection as a PAT tool would be further discussed.

In order to achieve the primary objective, the coater configuration (by using AAIs with different diameters) and process conditions were selected to induce different types of annular bed flow patterns without changing the fluidizing air flow rate. An acrylic product chamber was used to make sure that the annular bed flow pattern could be captured by a high speed camera. The fluidization status of the annular bed is determined by the pressure drop through the bed and the pressure drop is typically identical for the outer surface and interior of the annular bed (15). As such, the outer surface flow pattern is representative of the flow pattern of the whole bed. Particle image velocimetry (PIV) was used to interrogate high speed images of the annular bed and quantify annular bed flow patterns.

In order to achieve the secondary objective, color coating was carried out using the same coater configuration and process conditions as in annular bed flow pattern detection. In-process sampling during color coating and subsequent tristimulus colorimetry of the collected samples were employed to examine the effects of different annular bed flow patterns on particle coat uniformity. Nevertheless, particle recirculation within the partition column, particle mass flow rate and annular bed flow pattern can also be affected by changes of AAI diameter. Differences in particle coat uniformity may be the result of any combination of these three factors. Hence, the influences of confounding factors, i.e., the possible influences of particle recirculation within the partition column and mass flow rates, on coat uniformity have to be scrutinized and ruled out first before establishing the

relationship between annular bed flow patterns and particle coat uniformity. The relationship between AAIs and particle mass flow rates has been studied (16). However, the influence of AAIs on particle recirculation probability is still unknown and needs to be determined experimentally.

MATERIAL AND METHODS

Materials

Nonpareils (1.72 g/cm^3 density, 710–850 μm size fraction, Hanns G. Werner's, Tornesch, Germany) were used as the model particles. Hydroxypropylmethylcellulose (HPMC; Methocel E3-LV, The Dow Chemical, Midland, MI, USA) was used for both base-coating and production of white-colored seed particles for high-speed photography. Red color pigment (Opadry II, Colorcon, West Point, PA, USA) was employed to produce red-colored seed particles for high-speed photography and to color coat nonpareils.

Annular Bed Flow Pattern Detection

Production of Seed Particles and High-Speed Photography

Red-colored seed particles were produced by coating nonpareils to 2% weight gain using 10% w/w red pigmented aqueous suspension. White-colored seed particles were produced by coating nonpareils to 2% weight gain using 10% w/w HPMC solution. A binary mix of white (0.5 kg) and red (1.5 kg) seed particles was introduced into the transparent acrylic product chamber of the bottom spray fluid bed coater (Precision coater, MP-1, GEA Aeromatic-Fielder, Eastleigh, UK). The process parameters employed are listed in Table I. Air accelerator inserts of 20 mm (AAI-20), 24 mm (AAI-24) and 30 mm (AAI-30) diameters were selected for use to modulate air flow though the annular bed (Fig. 1-c). Image recording of the annular bed was carried out using a high-speed video camera (MotionPro HS-3, Redlake, Tallahassee, FL, USA). Recording speed used was 200 frames per second. Image size was set at 1,024 pixels by 1,280 pixels, and a total number of 1,000 frames were captured for each AAI used.

Particle Image Velocimetry and Post-Processing for Flow Visualization

PIV is one of the main quantitative methods for flow visualization (17). Although PIV was originally developed for fluid flow (18–21), this technique is increasingly being applied to the study of particulate flow (22–27). PIV involves capturing sequential images of the flow field and dividing them into sub-windows, from which velocity vectors are determined by means of sub-window roaming and pattern matching. The displacement between the original sub-window position and the best matched position in the following frame is considered the average displacement. Cross-correlation and minimum quadric difference (MQD) methods are the most commonly used methods to determine the extent of similarity between sub-windows (28).

MQD method was employed using Matlab (R2006b, The MathWorks, Natick, MA, USA) to perform PIV analysis due to its robustness (29). Quadric difference was calculated as follows (28):

$$C(\Delta X, \Delta Y) = \sum_{i=1}^{N}\sum_{j=1}^{N} \left| f_1(X_i, Y_j) - f_2(X_i + \Delta X, Y_j + \Delta Y) \right|$$

where X_i ,Y_j are the coordinates; ΔX, ΔY are the displacements along the coordinates, respectively; and f_1 and f_2 are the first and second images, respectively .

Post-processing of PIV results included generating streamlines for a clear picture of flow orientations using Matlab. The streamlines $s(x, y)$ are defined as curves that satisfy $dx/u = dy/v$, where u and v are the detected velocities along X and Y directions, and dx and dy are the curve derivatives along X and Y directions, respectively (30). Streamlines are curves that are instantaneously parallel to the velocity vectors produced by PIV.

Table I. Process Conditions for High-Speed Imaging and Color Coating

Process Parameters	Settings
Air flow rate	100 m^3/h
Inlet air temperature	70°C
Atomizing air pressure	2.0 bar
Partition gap	10 mm

Characterization of Coating Performance Using Color Coating and Tristimulus Colorimetry

Color Coating

Color coating and subsequent tristimulus colorimetry of in-process samples were used to assess coating performance under different annular bed flow patterns. Nonpareils were base-coated to 2% weight gain using 10% w/w HPMC in the Precision coater. A load of 2 kg base-coated particles were further color-coated to 2% weight gain using 10% w/w red pigmented aqueous suspensions. Process parameters used were the same as those employed during the high-speed imaging experiments, and spray rate was 10 g/min. Five in-process samples were taken for each 0.4% weight gain, and triplicate batches were color-coated for each AAI set-up.

Tristimulus Colorimetry and Statistical Analysis of Color Variance of In-Process Samples

Tristimulus colorimetry has been used to judge the appearance of color-coated tablets (31,32) as well as to estimate the coat uniformity of color-coated pellets (33). For the purpose of coat uniformity determination, the color intensity of spots on the particle surface is quantified in defined color spaces. The color difference (dE) between color-coated and white base-coated particles indicates the color intensity change on the particle surfaces, thus reflecting the amount of color pigment deposited on the particle surfaces. Hence, the variance of dE corresponds to the color variance of the sampled color-coated particles, and may be used as an inverse indicator of particle coat uniformity. For example, *F-test* has been used to compare the dE variances of

two sets of sampled color-coated particles for the purpose of comparing coat uniformity of particles coated using different types of coaters (5). Relative color variation (*RCV*), which is defined as the ratio of the standard deviation of *dE* to the mean of *dE*, expresses color variation relative to the magnitude of *dE* measurements. Hence, as used in the literature, *RCV* was preferably chosen for plotting the changes in relative color variation with increased weight gains (33).

Mathematically, under Commission Internationale de l'Eclairage (CIE) 1976 (L*, a*, b*) color space, *dE* between white (L_u, a_u, b_u) and color-coated particles (L_c, a_c, b_c) is calculated using Euclidean distance:

$$dE = \sqrt{(L_u - L_c)^2 + (a_u - a_c)^2 + (b_u - b_c)^2}$$

The mean color difference of n measured particles is expressed as $\overline{dE} = \frac{1}{n}\sum_{1}^{n} dE_i$, where dE_i is the color difference of the i^{th} measured particle.

RCV of n measured particles is expressed as

$$RCV = \frac{\sqrt{\frac{\sum_{i=1}^{n}\left(dE_i - \overline{dE}\right)^2}{n-1}}}{\overline{dE}} \times 100\%$$

A tristimulus colorimeter (Chroma Meter CR-241, Minolta, Osaka, Japan) with CIE standard illumination D_{65} was used to measure the color intensity of color-coated particles. For each sample, 200 particles were measured by determining the color intensity of a 0.3 mm diameter spot on the surface of each particle. In this study, mean *dE* was calculated after pooling *dE* measurements from triplicate batches (200 measurements for each sample per batch, hence, 600 measurements in total for each data point). The *RCV* of each batch was calculated separately. Consequently, for each weight gain, three *RCV* values were obtained from the triplicate batches for determination of mean *RCV* and inter-batch standard deviation of *RCV*. Mean *dE* and mean *RCV* plots were used to show the trends of inter-particle mean color difference and inter-batch relative color variation, respectively, with increased weight gains.

Two-sample *F-test* on variance using Matlab was performed to compare color variances of sample particles coated under different AAI settings. *F-test* rather than *t-test* was chosen in order to test the variance of *dE*, not the mean of *dE*. The null hypothesis of a two-sample *F-test* is that the two samples come from normal distribution with the same variance. *dE* values pooled from triplicate batches (600 *dE* values in total) were used in *F-test*, thus taking into account both inter-batch and inter-particle color variance.

Measurement of Particle Recirculation Probability Within Partition Column

As particle recirculation within the partition column was considered a major factor affecting coat uniformity, and the influences of AAIs on particle recirculation probability are not known, the particle recirculation probabilities of the three AAIs had to be checked before correlating annular bed flow pattern with coat uniformity. Fifty video clips of particle movement within the partition column were taken at a recording speed of 4,000 frames per second. The recirculation probabilities were derived from video clips using the method developed by Liew *et al.* (13). One-way ANOVA was then performed on the recirculation probabilities of the three AAI settings using Matlab.

RESULTS

Annular Bed Flow Patterns Classified

A sample high-speed image of the overall annular bed was given in Fig. 1-d. White particles were evenly distributed in the annular bed and strongly contrasted from the red (dark) particles, thus serving well as seed particles for PIV.

The PIV results of the annular bed flow patterns brought about by AAIs of three different diameters were shown in Fig. 2-a. With AAI-20 (Fig. 2-a-i), the air flow rate passing through the annular down-bed region was higher than when the other two AAIs were used. Intense bubbling fluidization was observed. Bubbles arose from the bed bottom, moved upwards and burst through the bed surface, scattering some particles into the air. Particles around the bubbles were recorded to move at a higher velocity than the rest. It was also observed that particles were transported from the bottom upwards to the top of the bed in the wake of each bubble. This flow pattern was termed "global fluidization" as the bubbles induced generalized particle movement and mixing in the annular bed. When AAI-24 was used (Fig. 2-a-ii), the air flow rate passing through the annular bed was lower, and bubbling fluidization was only observed in the lower region of the bed. The bubbles were smaller and dissipated upon reaching the middle of the bed. Hence, this flow pattern was named "localized fluidization." In contrast, AAI-30 induced a uniform, downward, "plug flow" in the annular bed (Fig. 2-a-iii); fluidization was not evident in this flow pattern.

Coat Uniformity of In-process Samples

Mean *dE* values of in-process samples were plotted in Fig. 3-a. Mean *dE* rose with coating weight gain but at a gradually decreasing rate. The increasing mean *dE* values were attributed to the increase in particle surface color intensity with more and more red color pigment being deposited on the particle surfaces. The leveling trend in the latter portion of the mean *dE* plot may be due to saturation of color pigment on the particle surfaces.

The *RCV* of in-process samples are shown in Fig. 3-b. As expected, an overall decreasing trend was observed for all three AAI settings, with increased coverage of the particle surfaces by the color pigment. Differences in *RCV* values of particles color-coated at the three AAI settings also decreased with increase in coat weight gain, and the differences may become negligible upon approaching complete coverage of the originally white particles by the color pigment. The influence of AAI settings on particle coat uniformity would be less important at higher weight gains with sufficient improvement in the coverage of the color coat.

F-test was used to compare the *dE* variances of color-coated particles for statistical comparison of particle coat uniformity in terms of inter-particle color variance. As shown in Table II, the *F-test* results on comparison of *dE* variances for the three AAI settings were consistent for 0.4%–1.2% weight

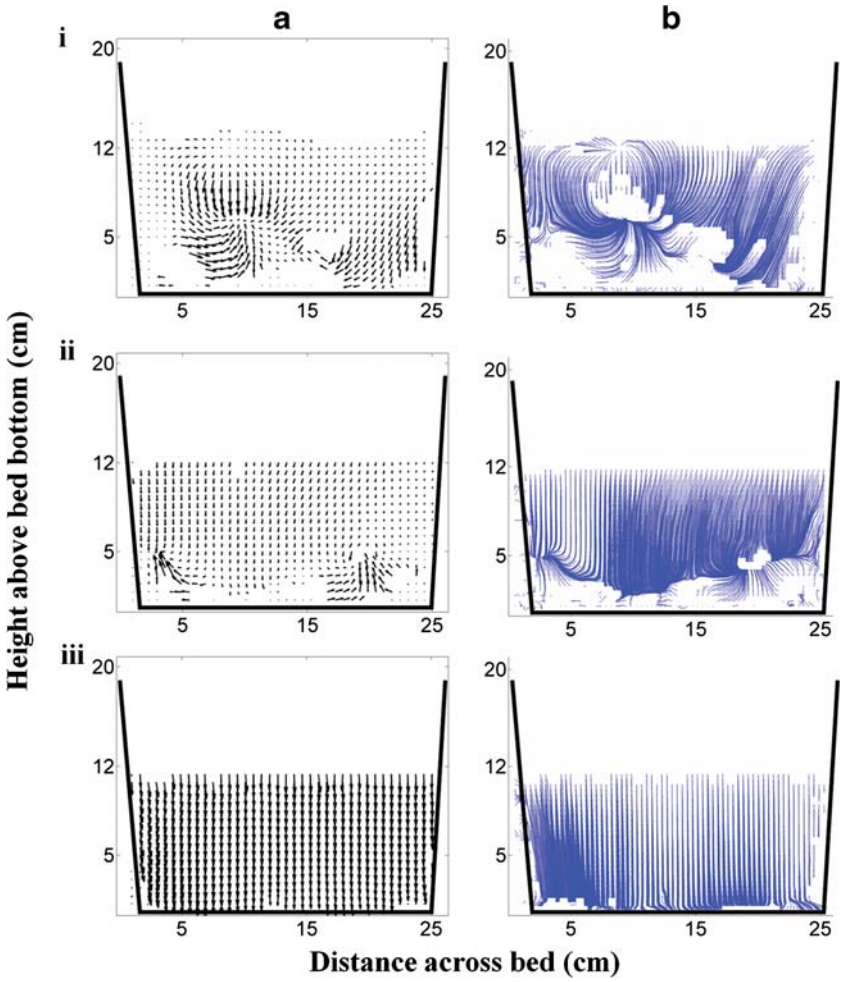

Fig. 2. (a) Sample PIV results of annular bed flow using (i) AAI-20, (ii) AAI-24 and (iii) AAI-30; (b) sample streamlines from PIV results using (i) AAI-20, (ii) AAI-24 and (iii) AAI-30.

gains. For instance, samples under AAI-30 had significantly lower *dE* variances than those under AAI-20 and AAI-24, while *dE* variances for AAI-20 and AAI-24 were not statistically significant. In contrast, the *F-test* results for the last two weight gains were neither consistent with one another nor with those of the first three weight gains. As coating is a layering process, the *F-test* results should, in theory, be consistent for all weight gains. Nevertheless, it is also known that the sensitivity of tristimulus colorimetry decreased with saturation of the color pigment on the particle surfaces (32). The observed inconsistency in *F-test* results for the last two weight gains may be attributed to decreased discrimination sensitivity induced by color saturation when coating reached weight gains higher than 1.2%. Statistical comparison of *dE* variances should thus be carried out on *dE* variances of color-coated particles with lower coat weight gains (i.e. up to the first three coat weight gains) for the following reasons: first, the impact of AAI settings on particle coat uniformity is expected to be greater at low coat weight gains and/or during the early stages of the coating process, and second, *dE* variances employed for statistical comparison should be within the sensitive detection range of the tristimulus colorimeter.

Consequently, based on *F-test* results and *RCV* trend of the first three weight gains, the color coats of particles coated at AAI-30 were found to have greater coat uniformity than those coated at AAI-20 and AAI-24, and the differences in *dE* variances were statistically significant. AAI-20 produced particles with higher degree of coat uniformity than those coated at AAI-24. Although the difference was not statistically significant, the trend in variance difference was consistently detected for the first two weight gains.

Particle Recirculation Probability Within the Partition Column

One-way ANOVA on particle recirculation probabilities of the three AAIs was not statistically significant ($p=0.4776$).

DISCUSSION

Influences of Particle Recirculation Within Partition Column and Particle Mass Flow Rate on Coat Uniformity

Although particle recirculation within the partition column is considered a major variability source, one-way ANOVA did not show statistically significant differences in particle recirculation probability for the three AAIs. Hence, the differences in coat uniformity observed within the scope of this study could not be attributed to particle recirculation within the partition column.

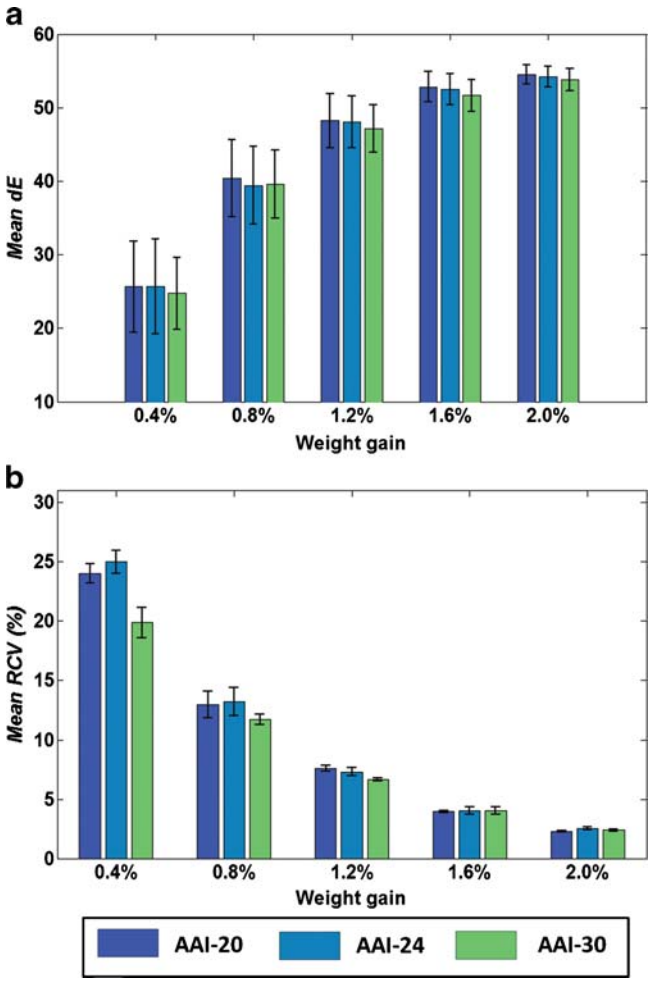

Fig. 3. (a) Trends of mean color difference (*dE*) and (b) mean relative color variation (*RCV*) of in-process samples obtained from AAI-20, AAI-24 and AAI-30.

For particle mass flow rate, AAI-20 was reported to induce the highest particle mass flow rate followed by AAI-24 and AAI-30 due to "Venturi" effect (16). According to the validated model developed by Turton *et al.*, higher mass flow rate within the partition column reduced cycle-time, and particles underwent more coating cycles through the spray zone, thus achieving more rapid attainment of uniform coat layers (2). For example, AAI-20 resulted in higher mass flow rate within the partition column than the other two AAIs, and AAI-24 generated higher mass flow rates than AAI-30; hence, the most uniform coat layer was expected from using AAI-20 followed by AAI-24 and "least" uniform from AAI-30. However, in this study, AAI-30 was found to produce particles with the best coat uniformity followed by AAI-20 and AAI-24, which was contradictory to the coat uniformity results predicted by mass flow rate.

Influence of Annular Bed Flow Patterns on Coat Uniformity

The particle coat uniformity trend could be better explained if the influence of annular bed flow pattern was taken into consideration. For a clearer picture of annular bed material flow orientations, streamlines were calculated from the velocity vectors and illustrated in Fig. 2-b.

Bubbles induced generalized mixing when AAI-20 was used (Fig. 2-a-i). Particles near the bubble head were pushed aside by the rising bubble. As a result, they moved downwards around the bubble and mixed with particles drawn in the wake of the bubble. With bubbles bursting through the annular bed surface, the particles on the bed surface were carried upwards into the air and subsequently fell back onto the annular bed. Moreover, it was observed that bubble generation spots were generally random at the base of the bed. Streamlines (Fig. 2-b-i) showed that generalized mixing was the main characteristic for this type of annular bed flow pattern. In this situation, particles from the bottom of the bed were brought upwards, against the general queue in the staging area for entry into the partition column for coating. This somewhat disrupted the orderliness of the coating process, resulting in a wider cycle-time distribution and hence a less favorable effect on coat uniformity.

Localized bubbling fluidization occurred when AAI-24 was used. The larger insert diameter of AAI-24 caused a decrease in air flow rate through the annular bed. This caused a lower pressure drop through the bed. The pressure dropped below the critical bubbling fluidization pressure in the middle of the bed, confining the bubbling fluidization to the bottom half of the annular bed. Streamlines derived showed that only the bottom half of the bed underwent fluidization (Fig. 2-b-ii). It was also observed that the bubbles were typically generated at the same vicinity, bringing some particles upwards to the middle of the bed. Upon dissipation of the bubbles, those particles that were lifted upwards by the bubbles moved downwards again as a result of gravity and circulation effects of particles entering the partition column. In the event that the particles encountered another developing bubble, their localized circulation path may yet be disrupted. As such, with localized fluidization, there was a tendency for a portion of particles to be confined to the bottom half of the annular bed, undergoing localized circulation but in effect isolated from the systematic coating cycles for an extended time. The localized fluidization stagnated particle flow near the product chamber wall but caused accelerated feeding in the near partition column region, resulting in a wider particle cycle-time distribution. Hence, this type of annular bed flow pattern can lead to relatively less uniform coating material deposition onto particle surfaces. Under the conditions tested, this adverse effect of localized fluidization may have suppressed the constructive effect of higher particle mass flow rate, resulting in a lower degree of coat uniformity for particles coated using AAI-24 than the rest of the AAIs.

Plug flow was observed when AAI-30 was used. This was associated with a further decrease in the air flow rate through the annular bed. Streamlines plotted showed uniform, downward particle movement without fluidization (Fig. 2-b-iii). This flow pattern was due to gravity and "Venturi" effect (16), which drew particles into the up-bed region via the partition column inlet. Under this flow pattern, freshly coated particles moved in pulsating rhythm smoothly and orderly via the staging annular bed for another coating cycle. This "queue system" ensured each particle underwent similar coating cycles and thus a narrow

Table II. Two-Sample *F-test* Results for *dE* Variance of In-Process Samples

Weight gain	*F-test* results (df_1=df_2=599 ,under χ^2-distribution)	Particles coated under AAI-20	Particles coated under AAI-24	Particles coated under AAI-20	Particles coated under AAI-30	Particles coated under AAI-24	Particles coated under AAI-30
0.4%	Variance of *dE*	38.5004	41.4601	38.5004	24.2068	41.4601	24.2068
	F	1.0768		1.5905		1.7127	
	p-value	0.3650		0.0000[a]		0.0000[a]	
0.8%	Variance of *dE*	27.4914	27.7351	27.4914	21.4154	27.7351	21.4154
	F	1.009		1.2837		1.2951	
	p-value	0.9140		0.0023[a]		0.0016[a]	
1.2%	Variance of *dE*	13.3606	12.4787	13.3606	10.5113	12.4787	10.5113
	F	1.0707		1.2711		1.187	
	p-value	0.4036		0.0034[a]		0.0360[a]	
1.6%	Variance of *dE*	4.3505	4.5537	4.3505	4.8100	4.5537	4.8100
	F	1.0467		1.1056		1.0563	
	p-value	0.5765		0.2194		0.5030	
2.0%	Variance of *dE*	1.6118	1.9761	1.6118	2.2882	1.9761	2.2882
	F	1.2261		1.4196		1.1579	
	p-value	0.0128[a]		0.0000[a]		0.0730	

[a] denotes significant statistical test result under significance level α=0.05.

particle cycle-time distribution. The influence of the "queue system" exceeded the negative effects of lower particle mass flow rate, producing particles with better coat uniformity than the other two AAIs.

However, if air flow rate passing through the annular bed was further decreased or there was insufficient load to maintain a uniform downward flow, motionless "dead" zones could occur at the bottom of the annular bed. "Dead" zones are highly undesirable, as a large portion of particles would then be isolated from systematic circulation without equal chances of entering the coating cycles. Hence, although plug flow can potentially confer superior coat uniformity, it is important to take precautions such that the operating process conditions are monitored to avoid conditions promoting "dead" zones at the bottom of the annular bed.

Significance of Annular Bed Flow Pattern

Three types of annular bed flow patterns were classified, and their influences on coat uniformity were assessed. As bottom spray fluid bed coating is a complex process, it was necessary to explore the extent of annular bed flow pattern's impact on particle coating and the factors governing the extent. The coat variance induced by cycle time distribution, which is mainly caused by the annular bed flow pattern in this study, can be estimated by the following equation (6):

$$Var_{coat} = \sqrt{\frac{Var(t)}{T \times E(t)}}$$

where Var_{coat} is the coat variance due to cycle-time distribution, *Var(t)* is the variance of particle cycle-time, *E(t)* is mean particle cycle-time and *T* is coating time. According to Cheng and Turton (6), the standard deviation of particle cycle-time, *Std(t)*, is proportional to *E(t)* , i.e. $Std(t) \approx 0.5E(t)$. Thus, the coat variance due to cycle-time distribution can be rewritten as $Var_{coat} \approx \sqrt{\frac{0.5Std(t)}{T}}$. Consequently, the influence of annular bed flow pattern depends on standard deviation of particle cycle-time *Std(t)* and coating time *T*.

In view of the analysis above, it is expected that the influence due to annular bed flow pattern would decrease with longer coating time (more coating cycles). Doubling coating time would decrease annular bed induced coat variance by about 30% (6). Therefore, the influence of annular bed flow pattern may be more evident in the following cases. The first case is low weight gain coating processes. For instance, for the purpose of reducing porosity, preventing dust formation during

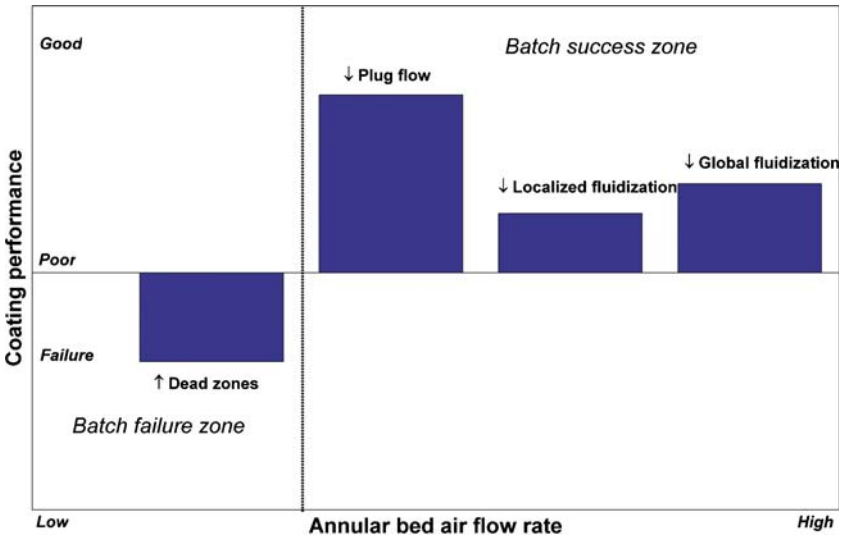

Fig. 4. Schematic representation of annular bed flow regimes with their influence on coating performance.

handling, decorative coating and certain sustained-release applications, the target coat thickness may be as thin as 5 μm (34). A coat layer of 5 μm is approximately equivalent to 1.1% weight gain for 1,000 μm particles. Second, the influences of annular bed flow patterns also depend on the solids content of the coating fluids as well as spray rate. Annular bed flow patterns tend to have greater influence in the case of high solids content coating fluids and high spray rates. For instance, 10% w/w coating fluid was used in this study; however, coating fluids of 20% w/w or higher may be used for coating. Organic solvent-based coating fluids can be sprayed at much faster spray rates than aqueous-based coating fluids (35). In such cases, annular bed flow patterns tend to exert greater influences on coat uniformity. Third, annular bed flow pattern is expected to have

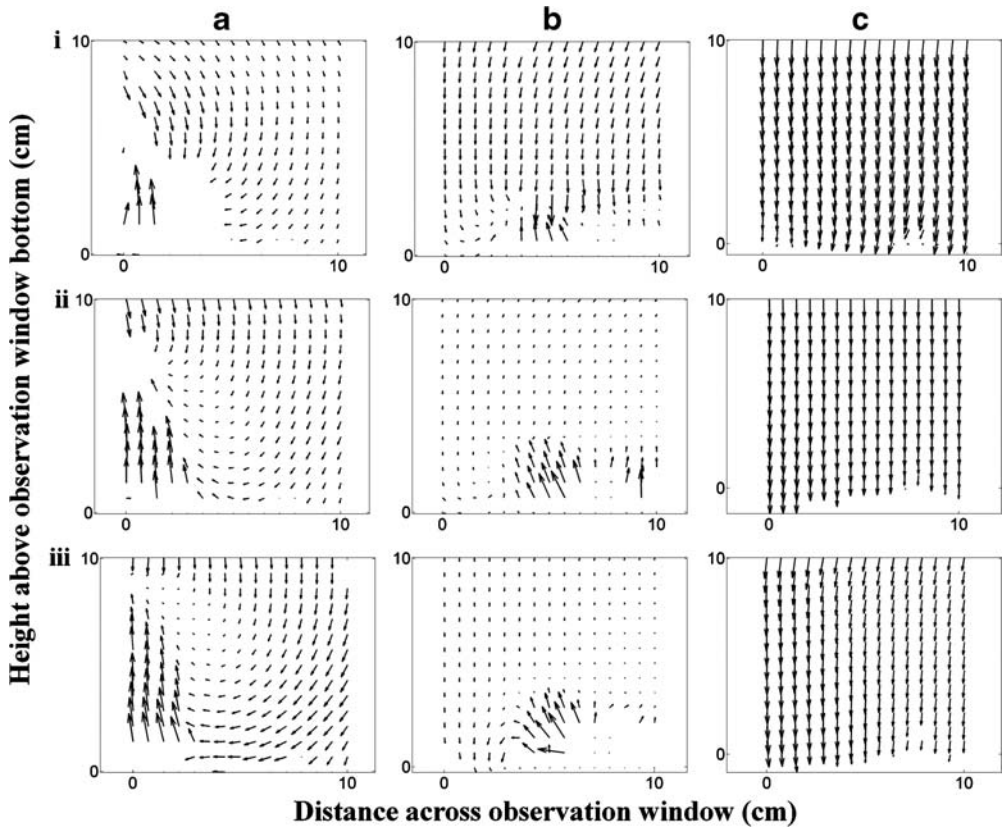

Fig. 5. PIV results from 10 cm by 10 cm observation window of (a) global fluidization, (b) localized fluidization and (c) plug flow at time point of (i) 0 ms, (ii) 20 ms and (iii) 40 ms.

greater impact in large-scale coaters where the particles have larger spaces to move about in when driven by rising bubbles, thus larger *Std(t)* values would be expected for a bubbling annular bed. Although a longer coating time may be used to counteract the negative influence of a bubbling annular bed, longer coating time and the use of more coating material would not be advantageous. Thus, for large-scale bottom spray fluid bed coating, it is desirable to monitor annular bed flow pattern to ensure that conditions are suitable for the presence of plug flow.

The capability of coating particles with a wider size distribution is another advantage of plug flow. Due to agitation and drag force of fluidization air, particles with a wide size distribution may segregate in the annular bed. In the case of segregation, larger particles tended to be less affected and remained in the bed surface region, while smaller particles were fluidized; therefore, larger particles are less likely to join the coating cycle, leading to non-uniform coat. If plug flow is present, the tendency for segregation can be avoided with the uniform, downward particle movement in the annular bed. Moreover, plug flow may also be helpful in controlling the development of electrostatic charges, as attrition is alleviated in the annular bed. For the purpose of summarizing the influences of different annular bed flow patterns on coat uniformity and to provide a general guidance on the coating process operation, a schematic qualitative representation of annular bed flow regimes *versus* their respective impact on coat uniformity was plotted (Fig. 4).

Feasibility of Monitoring Annular Bed Flow Pattern in Large-Scale Coating Process

As demonstrated in this study, the overall annular bed flow patterns could be visualized by using a transparent acrylic product chamber, and coating parameters adjusted to induce the desired annular bed flow pattern accordingly. Nevertheless, it is not practical to capture whole annular bed flow in a large-scale coater with a stainless steel product chamber. The observation window with a process monitoring camera would be the main mode to monitor annular bed flow pattern. With only a segment rather than the whole annular bed flow pattern visualized, it is necessary to investigate whether the overall flow pattern could be inferred from a limited local flow pattern detected through an observation window.

In this study, 10 cm by 10 cm window images were selected from the bottom of the original images, simulating images taken through an observation window in a large-scale coater. The

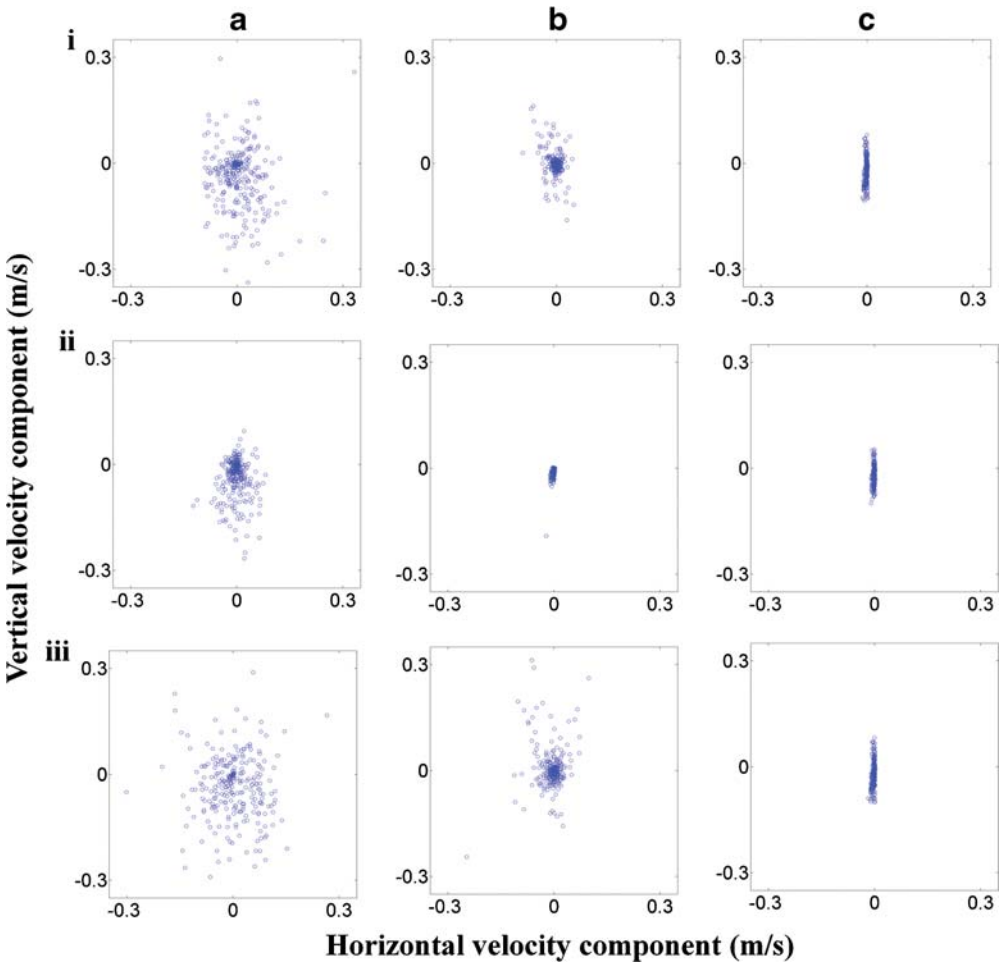

Fig. 6. Scatter plot of time series velocity vectors from three randomly chosen locations (i, ii and iii) under (a) global fluidization, (b) localized fluidization and (c) plug flow.

window images underwent the same image processing procedures as described earlier. The sample velocity vectors from the simulated observation window (Fig. 5) showed considerable differences for the three different types of flow patterns. For global fluidization (Fig. 5-a), velocity fields underwent drastic changes both in amplitude and orientation. For localized fluidization (Fig. 5-b), besides considerable orientation changes in a minority of the velocity vectors, most of the velocity vectors were observed to point downwards with small variations in amplitude. For plug flow, all the velocity vectors vary only in amplitude, indicating pulsed downward particle movement in the annular bed (Fig. 5-c).

In order to investigate how the characteristics of the different annular bed flow patterns could be further quantified, time series velocity vectors of three randomly chosen positions in the annular bed were employed as shown in Fig. 6. The horizontal vector component was plotted against the vertical vector component. For global fluidization, points scattered randomly on the plane, suggesting a random nature in both orientation and magnitude of particle movement. For localized fluidization, particle movement orientation was random, but the magnitude of particle movement was lower than that in global fluidization. The vertical velocity components showed the tendency of some particles to stagnate (Fig. 6-b-ii). This can be attributed to the dissipation of fluidization in the middle of the annular bed, inducing localized particle circulation in the lower annular bed. The localized particle circulation within the lower annular bed may block some particles from moving downwards, causing some particles to be motionless along the vertical direction for an extended time. This also further demonstrated the undesirable effect of localized fluidization. For plug flow, points were observed to locate near a vertically directed line, indicating uniform particle movement orientation (Fig. 6-c). It is also worthwhile to note that the randomness of particle movement generally decreased with an increase in AAI diameter. This is because with the increased AAI open area, less fluidization air passed through annular bed, causing more and more uniform particle motion in the annular bed.

In order to differentiate plug flow from the other flow patterns, standard deviation of the time series velocity orientation ($STSO$) was proposed to quantify the randomness of velocity orientation.

$$STSO = \sqrt{\frac{1}{n}\sum_{i=1}^{N}\left(\widehat{\theta}_i - \mu\right)^2}$$

where $\widehat{\theta}_i = \begin{cases} \theta_i & \text{for } \theta_i \le \pi \\ \theta_i - \pi & \text{for } \theta_i > \pi \end{cases}$ where θ_i was the i^{th} velocity orientation, $\widehat{\theta}_i$ was the i^{th} velocity orientation mapped to the region between 0 to π, and μ was the mean of mapped velocity orientation. This was based on the understanding that the orientation of plug flow was much more uniform than that of the other flow patterns.

Hence, plug flow was identified by images from the observation window and analysis of time series velocity orientation data. Moreover, white seed particles were used in this study mainly due to the need for a large area to be illuminated. Seed particles are not needed with intense local illumination over a small area in a practical application. In such cases, pulsed lighting synchronized with image capture may be advantageous. Thus, it is possible to use an observation window and a camera to monitor and ensure that a suitable annular bed flow pattern is present during a coating process. As such, a real-time annular bed flow pattern monitoring-based PAT tool could be developed.

CONCLUSION

Three types of annular bed flow patterns have been identified using PIV for bottom spray fluid bed coating process, and their influences on coat uniformity were determined by color coating and subsequent tristimulus colorimetry of in-process samples. Annular bed flow patterns were found to have considerable influence on coat uniformity. Plug flow gave the best coat uniformity, followed by global fluidization and localized fluidization. Moreover, plug flow was found to have the least tendency for segregation. Annular bed flow regime detection provided a general guidance for a good control of the coating process. Plug flow can be identified based on images from a simulated observation window. Flow patterns may be further quantified and classified by the variance of time series velocity orientations in a fixed location. Finally, the findings from this study demonstrated the feasibility and highlighted the potential of developing a real-time annular bed flow pattern monitoring-based PAT tool for large-scale bottom spray fluid bed coating.

ACKNOWLEGMENTS

The authors acknowledge the funding support from the National University of Singapore Academic Research Fund (R-148-000-085-112).

REFERENCES

1. Porter SC. Coating of tablets and multiparticulates. In: Aulton ME, editor. Aulton's pharmaceutics - the design and manufacture of medicines. New York: Churchill Livingstone; 2007. p. 500–14.
2. Crites T, Turton R. Mathematical model for the prediction of cycle-time distributions for the Wurster column-coating process. Ind Eng Chem Res. 2005;44:5397–402.
3. Saadevandi BA, Turton R. The application of computer-based imaging to the measurements of particle velocity and voidage profiles in a fluidized bed. Powder Technol. 1998;98: 183–9.
4. Tang ESK, Wang L, Liew CV, Chan LW, Heng PWS. Drying efficiency and particle movement in coating–Impact on particle agglomeration and yield. Int J Pharm. 2008;350:172–80.
5. Heng PWS, Chan LW, Tang ESK. Use of swirling airflow to enhance coating performance of bottom spray fluid bed coaters. Int J Pharm. 2006;327:26–35.
6. Cheng X, Turton R. The prediction of variability occurring in fluidized bed coating equipment. I. The measurement of particle circulation rates in a bottom-spray fluidized bed coater. Pharm Dev Technol. 2000;5:311–22.
7. Sudsakorn K, Turton R. Nonuniformity of particle coating on a size distribution of particles in a fluidized bed coater. Powder Technol. 2000;110:37–43.
8. Turton R. Challenges in the modeling and prediction of coating of pharmaceutical dosage forms. Powder Technol. 2008;181: 186–94.
9. KuShaari K, Pandey P, Song Y, Turton R. Monte Carlo simulations to determine coating uniformity in a Wurster fluidized bed coating process. Powder Technol. 2006;166:81–90.

10. Yu LX. Pharmaceutical quality by design: product and process development, understanding, and control. Pharm Res. 2008;25:781–92.
11. Palmer SE, Seville JPK, Ingram A, Fitzpatrick S, Fan X. Tracking particle motion in a Wurster coater using positron emission, Fifth World Congress on Particle Technology (Session #158b) on 2006 AIChE Spring National Meeting. Orlando: American Institute of Chemical Engineers; 2006.
12. Bi X, Pugsley T. Investigation of the sources of variability in the Wurster coater: analysis of particle cycle times using PEPT. In: Berruti F, editor. 2007 ECI Conference on The 12th International Conference on Fluidization—New Horizons in Fluidization Engineering. Vancouver: The Berkeley Electronic Press; 2007. p. 431–40.
13. Liew CV, Wang LK, Heng PWS. Development of a visiometric process analyzer for real-time monitoring of bottom spray fluid-bed coating. J Pharm Sci. 2010;99:346–56.
14. Christensen FN, Bertelsen P. Qualitative description of the Wurster-based fluid-bed coating process. Drug Dev Ind Pharm. 1997;23:451–63.
15. Rhodes M. Fluidization. Introduction to particle technology. New York: Wilety; 1998. p. 97–110.
16. Chan LW, Tang ESK, Heng PWS. Comparative study of the fluid dynamics of bottom spray fluid bed coaters. AAPS PharmSciTech. 2006;7:37–64.
17. Smits AJ, Lim TT. Flow visualization: techniques and examples. River Edge: Imperial College Press; 2000. p. 2–26.
18. Adrian RJ. Particle-imaging techniques for experimental fluid mechanics. Annu Rev Fluid Mech. 1991;23:261–304.
19. Keane RD, Adrian RJ. Theory of cross-correlation analysis of PIV images. Appl Sci Res. 1992;49:25.
20. Westerweel J. Fundamentals of digital particle image velocimetry. Meas Sci Technol. 1997;8:1379–92.
21. Westerweel J. Digital particle image velocimetry: theory and application, Ph.D thesis, Technische Universiteit Delft, Delft, Netherlands; 1993. p. 236
22. Conway S, Lekhal A, Khinast J, Glasser B. Granular flow and segregation in a four-bladed mixer. Chem Eng Sci. 2005;60:7091–107.
23. Darelius A, Lennartsson E, Rasmuson A, Niklasson Bjorn I, Folestad S. Measurement of the velocity field and frictional properties of wet masses in a high shear mixer. Chem Eng Sci. 2007;62:2366–74.
24. Duursma GR, Glass DH, Rix SJL, Yorquez-Ramirez MI. PIV investigations of flow structures in the fluidised bed freeboard region. Powder Technol. 2001;120:2–11.
25. Nilpawar A, Reynolds G, Salman A, Hounslow M. Surface velocity measurement in a high shear mixer. Chem Eng Sci. 2006;61:4172–8.
26. Ostendorf M, Schwedes J. Application of particle image velocimetry for velocity measurements during silo discharge. Powder Technol. 2005;158:69–75.
27. Slominski C, Niedostatkiewicz M, Tejchman J. Application of particle image velocimetry (PIV) for deformation measurement during granular silo flow. Powder Technol. 2007;173:1–18.
28. Suh YK. Multi-frame MQD-PIV. KSME Int J. 2003;17:1552–62.
29. Mori N, Chang K-A. Introduction to MPIV—user reference manual. http://www.oceanwave.jp/softwares/mpiv (accessed September 2009).
30. Nakayama Y, Boucher RF. Introduction to fluid mechanics. New York: Wiley; 1999. p. 42.
31. Cole G, Aulton ME, Hogan JE. Pharmaceutical coating technology. Bristol: Taylor & Francis; 1995. p. 1–5.
32. Wirth M. Instrumental color measurement— method for judging the appearance of tablets. J Pharm Sci. 1991;80:1177–9.
33. Chan LW, Chan WY, Heng PWS. An improved method for the measurement of colour uniformity in particle coating. Int J Pharm. 2001;213:63–74.
34. Lehmann K. Coating of multiparticulates using polymeric solutions—formulation and process considerations. In: Ghebre-Sellassie I, editor. Multiparticulate oral drug delivery. New York: Marcel Dekker; 1994. p. 51–76.
35. Fukumori Y. Coating of multiparticulates using polymeric dispersions—formulation and process considerations. In: Ghebre-Sellassie I, editor. Multiparticulate oral drug delivery. New York: Marcek Dekker; 1994. p. 79–111.